

JOINING OF CARBON STEEL AISI 1006 TO ALUMINUM ALLOY AA6061-T6 VIA FRICTION SPOT JOINING TECHNIQUE

Munaf Hashim RIDHA

Engineering Technical College - Baghdad, Middle Technical University, Baghdad, IRAQ

Mursal Luaibi SAAD

Technical Institute - Suwaira, Middle Technical University, Baghdad, IRAQ

Isam Tareq ABDULLAH

Engineering Technical College - Baghdad, Middle Technical University, Baghdad, IRAQ

Osamah Sabah BARRAK

Institute of Technology - Baghdad, Middle Technical University, Baghdad, IRAQ

Sabah Khammass HUSSEIN*

Engineering Technical College - Baghdad, Middle Technical University, Baghdad, IRAQ

E-mail: sabah.kh1974@yahoo.com

Abbas Khammas HUSSEIN

Materials Engineering Department, University of Technology, Baghdad, IRAQ

This work aims to join sheets of carbon steel to aluminum alloy AA6061. A lap joint arrangement was used with a joint lap area of dimensions $25 * 25 \text{ mm}$. The joining procedure was carried out using a rotating tool of 10 mm shoulder diameter. Three process parameters, with three levels for each parameter, were selected to investigate their effects on joints quality. The parameter's levels for each experiment were designed using the design of the experiment method (DOE). The results indicated that the two materials were joined by a mechanical interlock at an interface line, without formation of intermetallic compounds. The shear force of the joint reached an ultimate value of 4.82 kN . The shear force of the joint improved by increasing plunging depth of the tool. Samples of minimum shear force value failed by a pull-outting aluminum metal from the carbon steel specimen. Samples of higher shear force value exhibited a shear mode of fracture. Increasing the rotating speed and decreasing pre-heating increased the process temperature.

Key words: friction spot, joining, AA6061, carbon steel AISI 1006, DOE.

1. Introduction

Friction stir spot welding (FSSW) is a solid-state welding technique [1] that offers various advantages such as excellent mechanical properties, negligible distortion, low residual stresses and few weld defects [2]. Porosities and lack of fusion were considered the major defects found in the conventional welding process [3,4]. The FSSW technique is utilized to weld similar and dissimilar materials. The FSSW method was used in the automotive, rail vehicle construction, aerospace industry, and electrical industry [5, 6] instead of riveting techniques, which reduced weight and energy consumption [7]. This method was used to join different materials such as aluminum alloys to carbon steel [8]. In this work, the results indicated that an Fe/Al

* To whom correspondence should be addressed

intermetallic compound (IMC) layer formed at an interface line between the two materials. A pin-less FSSW technique is equivalent to that of the conventional FSSW, in which the welding method consists in plunging a pin-less tool into the upper surface of a sheet metal, with a stirring for a short dwell time and retreating [9].

Pure copper (Cu) and carbon steel (CS) sheets were welded using the FSSW process. It was found that maximum shear force reached a value of 4560 N at 1800 RPM , 0.4 mm plunge depth and pre-heating [10]. The effect of material positions was studied in the FSSW using two materials of aluminum alloys: AA5052-AA6063. Fracture loads of the peel test indicated that the load increased when the AA6063 sheet was put over the AA5052 sheet [11]. Dissimilar materials of AA5754 and AA6061 were welded by the FSSW. The results showed a significant effect of rotational tool speed on the tensile shear force of the joints. The maximum tensile shear force reached a value of 6.060 kN at a rotating speed of 1000 RPM and feed rate of 0.04 mm/s [12]. AA5058-H116 aluminum alloy was welded by the FSSW with various rotational speeds and dwell times. The results indicated that the Vickers hardness of welded samples exhibited a maximum value at the following conditions: rotating speed of 900 RPM and a dwell time of 5 s [13]. AA2024-T3 and AA7075-T6 sheets were welded using the FSSW using a tool with a rotating speeds range of $600 - 1400\text{ rpm}$ and plunge depths range of $0.1 - 0.5\text{ mm}$, with different media. An increase in the rotating speed and plunge depth values led to increase the tensile shear force of the joints. Optimum tensile shear forces were 5900 and 6700 N at ambient and underwater welds, respectively [14]. AA2014 and AA7075 were welded using the FSSW with different welding parameters. The welded joints showed a higher tensile strength of 214 MPa and tensile shear force of 6 kN at a rotating speed of 1000 RPM , feed rate of 45 mm/min and 2° tool tilt angle [15]. The effect of pin length and penetration depth on joint's quality was studied. The FSSW process was used to weld different materials of AA6063 and galvanized low carbon steel. Ultimate loads of the joints raised by increasing penetration of the tool and decreasing the pin length. The fracture mode showed an interfacial mode, which changed to a circumferential mode when the tool penetration depth went up, and the pin length decreased [16].

Low carbon steel was welded by the FSSW using double side adjustable flat tools. All defects that the generated by the conventional FSSW, such as hook shape and keyhole, were eliminated. Joint performance improved in the case of a plug fracture mode. Maximum shear tensile force increased to a value of 23 kN [17]. The effect of penetration depth and tool geometry on mechanical properties of joints of type AA5052 to low carbon steel was analyzed. The fracture force of the welded samples improved by increasing the tool's penetration depth. Optimization of the tool geometry, also, raised the fracture force of the welded samples [18]. Similar and dissimilar joints of two materials, AA6061-T6 and Cu, were welded by the FSSW with single and multi- spots using a pin-less tool. Fractured surfaces showed numerous dimples throughout the surface in similar joints. Dissimilar materials joints exhibited micro-cracks at fractured surfaces [19]. The influence of rotating speed and tool pin geometry on mechanical properties and microstructure evolution of AA 5052-H112 FSSW joint was studied. A cylindrical pin exhibited a higher strength of welds compared to a step pin. Increasing the rotating speed of the tool raised strength of the joints. The welded joints using a cylindrical pin tool exhibited maximum values of tensile shear of 3589 N and cross-tension loads of 3419 N at 1400 RPM . Two types of fracture modes are observed: de-bonding and pull-out of nugget fractures [20]. However, welding of similar and dissimilar materials using the friction stir technique may reduce the joint strength due to the stress concentration generated from the pin trace.

In this study, carbon steel (1006-AISI) was welded together with AA6061-T6 using the friction spot technique by a flat tool (without pin). The influence of plunging depth, rotating speed, and pre-heating on the shear tensile force of joints was investigated. The welding process parameters were analyzed by the design of the experiments method. Microstructure of the joints was examined.

2. Experimental procedure

2.1. Materials

Sheets of aluminum alloy AA6061-T6 and carbon steel 1006-AISI were used for the welding process. The thickness of AA6061-T6 and carbon steel 1006-AISI sheets were 1.6 mm and 1 mm , respectively.

Chemical compositions and mechanical properties for both materials are listed in Tabs 1, 2 and 3. The sheets were prepared with dimensions of $100 * 25 \text{ mm}$ [21], as shown in Fig.1.

Table 1. Chemical composition of AA6061-T6.

Element wt. %	Si	Fe	Cu	Mn	Mg	Cr	Zn	Ti	Al
ASTMB209	0.4-0.8	0.7	0.15-0.4	0.15	0.8-1.2	0.04-0.35	0.25	0.15	Bal.
Measured	0.593	0.405	0.231	0.102	0.87	0.180	0.021	0.056	Bal.

Table 2. Chemical composition of 1006 AISI.

Element wt. %	C	Mn	P	S	Fe
ASTM A830M	≤ 0.080	0.25-0.4	≤ 0.040	≤ 0.050	Bal.
Measured	0.062	0.369	0.016	0.006	Bal.

Table 3. Mechanical properties of the materials.

Material	σ_u (MPa)	σ_y (MPa)
AA6061-T6	348	254
1006 AISI	235	136



Fig.1. Aluminum and carbon steel sheets.

2.2. Joining process

The experiments were carried out in three steps: arranging, fixing and joining the specimens. In the first step, the specimens were placed with a lap joint configuration of a lap area of $25 * 25 \text{ mm}^2$. The steel specimen was put over the aluminum specimen, as illustrated in Fig.2.

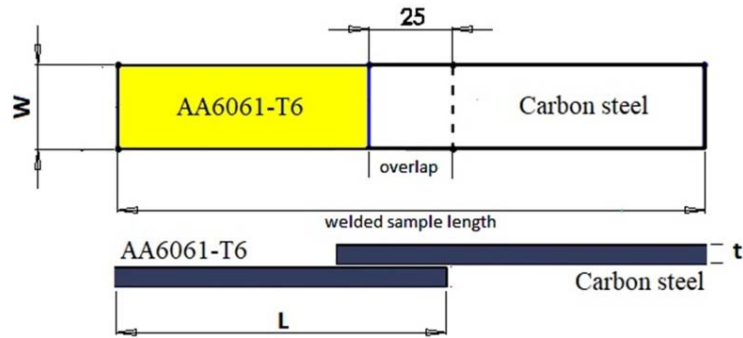


Fig.2. Lap joint arrangement.

The second step consisted in fixing the lap joint configuration of the sample on the machine base to avoid slipping of the specimens through the joining process. A carbon steel material was used to manufacture elements of sample fixture. The fixture consisted of three parts: bolts, upper and lower plates. The lower plate was manufactured, including a slot to contain the sample, with the same width of the specimens. The main job of the slot was to prevent the sample from slipping during the joining process. The lower plate was fixed at the machine base with suitable fixing bolts. The upper plate (cover) is put over the lower plate to fix the sample, with suitable fixing bolts, as shown in Fig.3. A tool of a cylindrical shape was produced from a tungsten carbide material to perform the joining. The tool was prepared with a shoulder diameter of 10 mm and a length of 80 mm . A vertical milling machine was used to carry out the joining process.

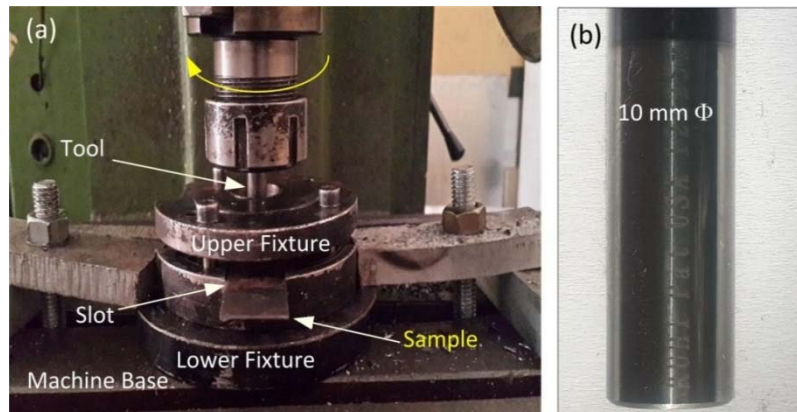


Fig.3. (a) Fixture assembly; (b) Tool.

The joining step included three stages: pre-heating, plunging and drawing-out the tool, as shown in Fig.4. Initially, the tool rotates and touches the upper surface of the carbon steel plate during a period of time to pre-heat (soften) the carbon steel material under the shoulder surface. At the end of the pre-heating time, the rotating tool moves down to plunge through the carbon steel specimen with a plunging depth. This stage is carried out by applying force from the machine on the sample at the contact area between the shoulder surface and the upper surface of the carbon steel specimen. At the end of this stage, joining of the two materials is achieved, and the tool is moved upward to finish the joining process. The joint exhibits a tool trace at the upper surface of the carbon steel sample, as illustrated in Fig.4c.

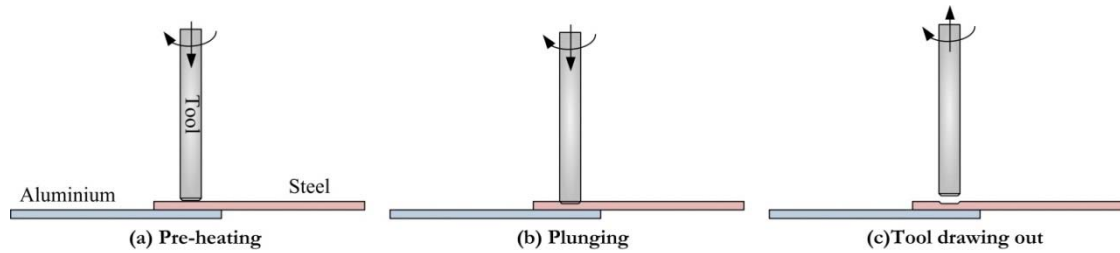


Fig.4. Joining stages.

2.3. Joining parameters

Three process parameters were utilized to analyze their influence on joint quality: rotating speed, pre-heating time, and plunging depth of the tool. Three levels were used for each process parameter. The design of the experiment approach (DOE) was utilized to design the levels of the parameters for each experiment, with the assistance of the Minitab program. Accordingly, nine experiments were designed, as listed in Table 4.

Table 4. Levels of process parameters.

No.	Rotating Speed (RPM)	Pre-Heating Time (Second)	Plunging Depth (mm)
1	1120	5	0.2
2	1120	10	0.4
3	1120	15	0.6
4	1400	5	0.4
5	1400	10	0.6
6	1400	15	0.2
7	1800	5	0.6
8	1800	10	0.2
9	1800	15	0.4

2.4. Microstructure test

To inspect the microstructure of the joints along the interface boundary, the microstructure test is carried which contains the following steps: cut the welded sample at the lap-joint cross-section and insert it through a cylindrical mounting. For metallographic specimen preparation, papers of silicon carbide grinding of degree 400,600,800,1200 and 2000 were used with a rotating speed of 2000 RPM, with the aid of a universal polishing and grinding machine. Water was used as a cooling liquid throughout the grinding process. After the grinding stage, the polishing stage began immediately, which involved the use of polishing cloth, alumina (Al₂O₃) and disc rotating speed. After the polishing stage, the etching stage began, which included immersing the specimen in an etching solution (1-5mL HNO₃ and 100mL ethanol of 95%) for the carbon steel specimen, and a solution (2mL HF, 3mL HCL, 5mL HNO₃, and 190mL water) for the aluminum specimen for a few seconds. The sample was washed with water and dried with hot forced air [22].

3. Results and discussion

3.1. Shear force of the joint

A shear force test was carried out on the joined samples to validate joint quality and examine the effect of the process parameters on the shear force of the joint. Figure 5 shows a variation of the joint's shear force for each

sample. Each sample was tested three times; an average value was taken into account. The shear force of the joints exhibited lowest and highest shear force value of 3.31 and 4.82 kN in samples No.9 and 5, respectively.

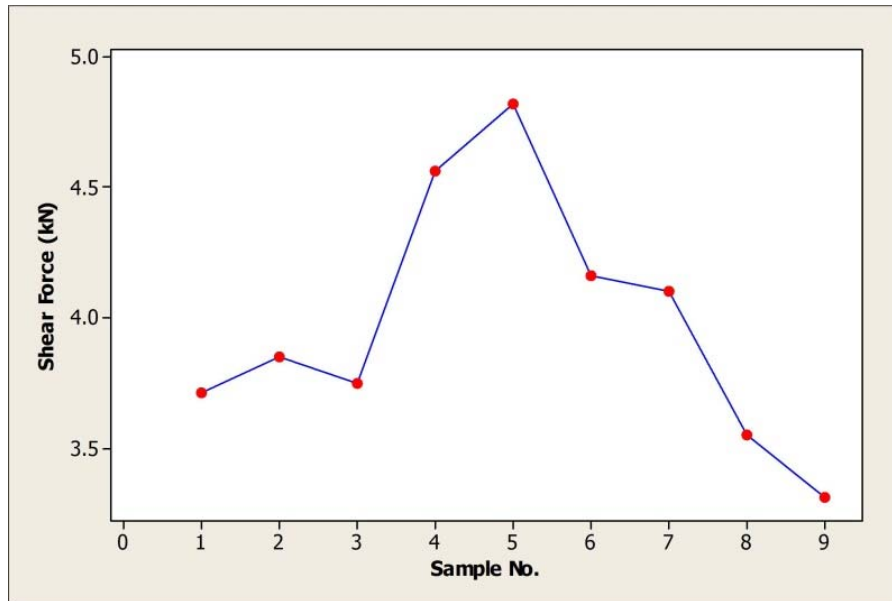


Fig.5. Shear forces of samples.

The joint shear forces were analyzed using the DOE, as illustrated in Fig.6. The main effect plot, Fig.6a, displayed that the shear force of the joint increases by increasing the plunging depth of the tool and decreasing the pre-heating time [23]. This can be due to the fact that an increase in the plunging depth can increase the interlock at the joint surface between the two materials with the aid of the applied pressure of the tool. The Pareto chart indicated that the shear force of the joint is highly affected by the plunging depth of the tool, followed by the pre-heating time and the rotating speed of the tool [24].

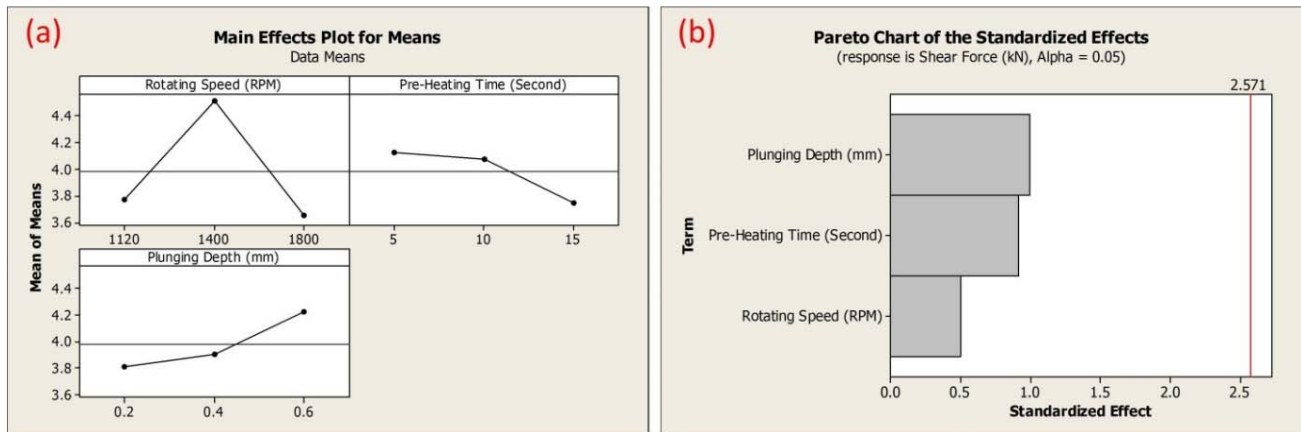


Fig.6. Analysis of shear force by DOE (a) main effect plot; (b) Pareto chart.

Moreover, a simple formula of the shear force of the joint, as a function of the process parameters, was estimated as follows:

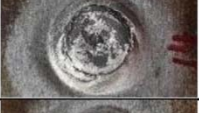
$$S = 4.38775 - 3.07078E - 04V - 0.0383333T + 1.04167H \quad (3.1)$$

where S is shear force (kN), V is the rotating speed (RPM), T is the pre-heating time (second), H is the plunging depth (mm).

3.2. Joint's surface feature

Table 5 illustrates surface features of each sample. The first column shows the lower surface of the aluminum specimen. Most of the samples showed that the aluminum metal (under the tool shoulder) exhibited a spiral shape under the effect of a higher applied load and heat input. This indicates that the aluminum metal reached the solid state during the joining process. The second column shows the upper surface of the steel specimen which contained a tool trace. The third column shows the fractured surface of the aluminum specimen at a common region between the two materials. The fractured surface of the samples, No.1, 2, 3, and 9, exhibited the minimum value of the shear force of the joint and failed by pull-outing of the aluminum metal from the carbon steel specimen. The samples that presented a higher shear force of the joint failed by shearing the aluminum metal at the contact area (as shown in the sample No.5).

Table 5. Surface features of the samples.

No.	Aluminum	Steel	Aluminum
	Outer surface	Outer surface	Inner surface
1			
2			
3			
4			
5			
6			
7			
8			
9			

3.3. Process temperature

During the joining process, maximum temperature for each sample was recorded and plotted in Fig.7. The process temperature reached lowest and highest values at joining of the samples No.3 and 7, with values of 195 and 295°C , respectively. Regardless of the pre-heating time and plunging depth of the rotating tool, the samples No.3 and 7 were joined at a minimum and maximum rotating speed. So, raising the rotating speed of the tool increased the process temperature [25]. This can be due to the fact that an increase in the rotating speed increases the rotating friction between the shoulder surface and the upper surface of the carbon steel specimen.

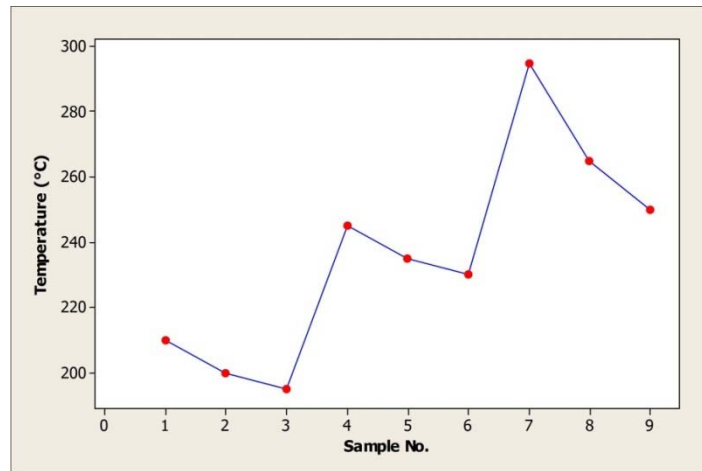


Fig.7. Maximum temperature for each sample.

The effect of the process parameters was analyzed using the DOE, as illustrated in Fig.8. The Pareto chart, Fig.8a, shows that the rotating speed of the tool had the most significant effect on the process temperature [26], followed by pre-heating time and plunging depth of the tool. The main effect plot indicated that the process temperature increased by increasing the rotating speed and decreasing the pre-heating time. Increasing the pre-heating time can increase the amount of solidification of the upper surface of the steel specimen, which reduces the friction between this surface and the shoulder surface. So, the process temperature decreased with increasing the pre-heating time.

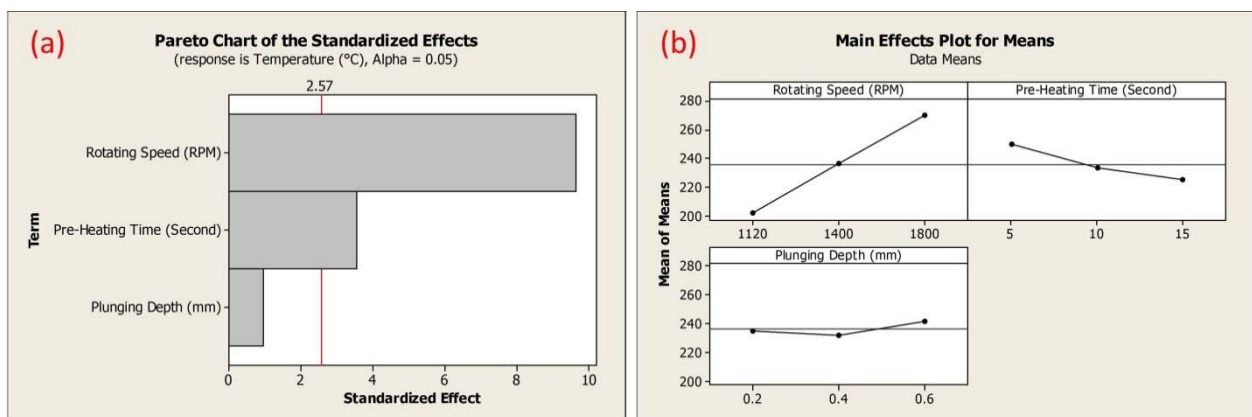


Fig.8. Analysis of process temperature by DOE (a) main effect plot; (b) Pareto chart.

3.4. Joint's microstructure

A joint cross-section of the sample No.5 was prepared to examine microstructure behavior along the interface boundary, as shown in Fig.9. The joint cross-section indicated that both materials were thermally deformed due to higher load applied and heat input [27]. The steel region deformed highly compared with the aluminum. The upper surface of the steel deformed with a tool trace shape containing a hook at the tool trace boundary. An interface between the two materials can be observed, as shown in Fig.9 (images 5 and 6), at the interface line between the two materials. The microstructure images indicated that the two materials joined at the interface line without the presence of defects, cracks, voids or gaps. The carbon steel material reached the solid-state, as shown in Fig.9 (6). The carbon steel metal flowed, under the effect of tool load that stirred the metal, below the tool shoulder. Due to the maximum input heat and load applied through the joining process, the aluminum side exhibited fine grain size.

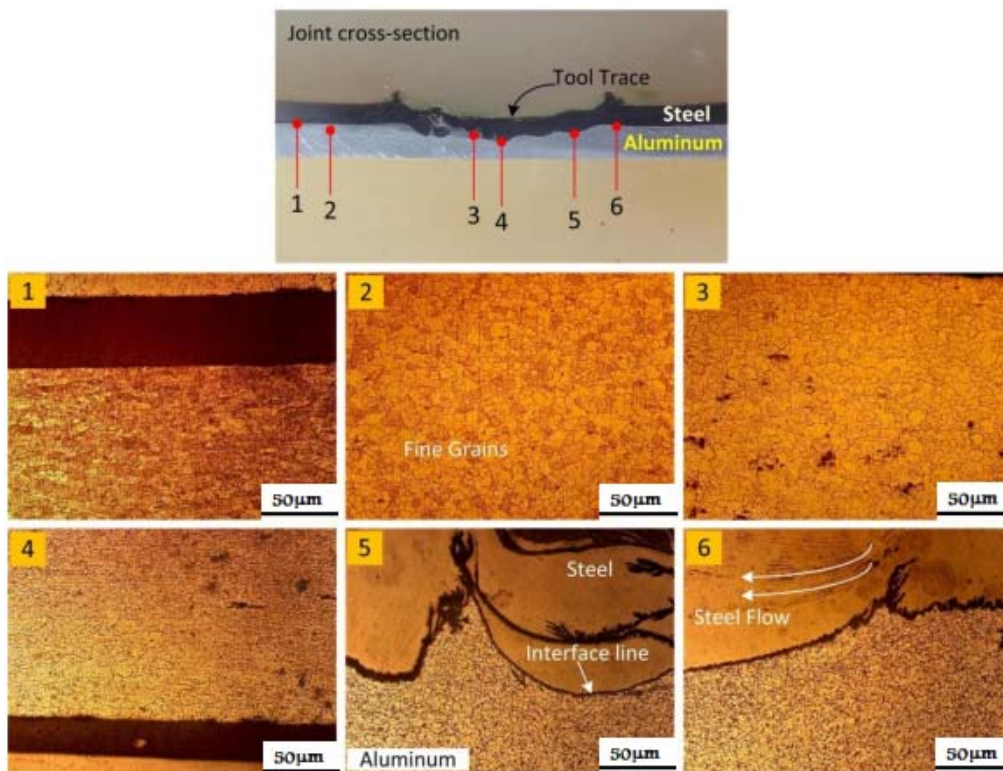


Fig.9. Microstructure of joint cross-section, sample No.5.

3.5. Energy Dispersive Spectroscopy (EDS)

EDS inspection was performed on sample No.5 at the interface line of the two materials to analyze the joining mechanism at the interface line, as illustrated in Fig.10. Map image indicated that the aluminum metal spread through the carbon steel pores and joined with no defects. The two materials joined at the interface line of a micron scale. The spectrum map indicated that the interface line included chemical elements without intermetallic compounds (IMCs). The aluminum and iron elements exhibited higher peaks compared with other elements. So, the two materials were joined by a mechanical interlock at the interface line without the formation of IMCs.

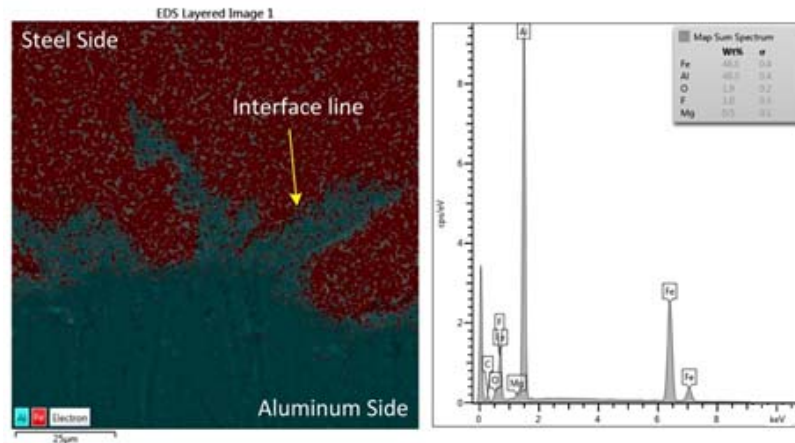


Fig.10. Interface line EDS analysis, sample No.5.

4. Conclusion

1. The shear force of the joint increased by increasing the plunging depth of the tool and decreasing the pre-heating time.
2. The plunging depth of the tool was the most influential factor affecting the shear force of the joint, followed by the pre-heating time and the rotating speed of the tool.
3. Samples No.1, 2, 3, 8 and 9, of the smallest shear force of the joint, failed by pull-outting the aluminum metal from the carbon steel at the joined region.
4. A shear mode of fracture was observed at the samples No.4, 5, 6 and 7 that exhibited the higher shear force of the joint .
5. The rotating speed of the tool was the most influential factor affecting the process temperature.
6. The process temperature increased with increasing and decreasing the rotating speed to *1800 RPM* and pre-heating time to *5 sec* , respectively.
7. The two materials joined by a mechanical interlock without the presence of defects such as gaps, cracks or voids and without formation of intermetallic compounds.
8. The two materials joined at the interface line, with a width of a micron scale.
9. The higher load and/or heat input refined the material's grain at the joint cross-section.
10. The aluminum metal penetrated through the carbon steel pores at the interface line.

Acknowledgement

The authors would like to thank the heads of the applied mechanical Engineering department, Engineering Technical College - Baghdad, Middle Technical University, and all teaching staff of the department for their assistance.

Nomenclature

- AA* – aluminium Alloy
DOE – Design of Experiments
FSSW – friction stir spot welding
IMC – intermetallic compound
CS – carbon steel

<i>Al</i>	– aluminium
<i>Cu</i>	– copper
<i>RPM</i>	– revolutions per minute
<i>LCS</i>	– low carbon steel
<i>AISI</i>	– American Iron and Steel Institute
<i>mm</i>	– millimeter
<i>kN</i>	– kilonewton
σ_y	– yield strength
σ_u	– ultimate tensile strength
<i>EL</i>	– elongation
<i>MPa</i>	– megapascal
<i>L</i>	– length
<i>W</i>	– width
<i>t</i>	– thickness
<i>WZ</i>	– welding zone

References

- [1] Suryanarayanan R. and Sridhar V. G. (2021): *Studies on the influence of process parameters in friction stir spot welded joints – A review.*– Materials Today: Proceedings, vol.37, No.2, pp.2695-2702, doi.org/10.1016/j.matpr.2020.08.532.
- [2] Tozaki Y., Uematsu Y. and Tokaji K. (2010): *A newly developed tool without probe for friction stir spot welding and its performance.*– Journal of Materials Processing Technology, vol.210, No.6, pp.844-851, doi.org/10.1016/j.jmatprotec.2010.01.015.
- [3] Pandey A. K. and Mahapatra S. S. (2019): *Investigation of weld zone obtained by friction stir spot welding (FSSW) of aluminium-6061 alloy.*– Materials Today: Proceedings, vol.18, No.7, pp.4491-4500, doi.org/10.1016/j.matpr.2019.07.419.
- [4] Abdullah I.T., Ridha M.H., Barrak O.S., Hussein S.K. and Hussein A.K. (2021): *Joining of Aa1050 sheets via two stages of friction spot technique.*– Journal of Mechanical Engineering Research and Developments, vol.44, No.4, pp.305-317.
- [5] Liu F. C., Hovanski Y., Miles M. P., Sorensen C. D. and Nelson T. W. (2018): *A review of friction stir welding of steels: Tool, material flow, microstructure, and properties.*– Journal of Materials Science & Technology, vol.34, No.1, pp.39-57, doi.org/10.1016/j.jmst.2017.10.024.
- [6] Bagheri B., Abbasi M., Abdollahzadeh A. and Omidvar H. (2020): *Advanced approach to modify friction stir spot welding process.*– Metals and Materials International, vol.26, No.10, pp.1562-1573, doi.org/10.1007/s12540-019-00416-x.
- [7] Xiong J., Peng X., Shi J., Wang Y., Sun J., Liu X. and Li J. (2021): *Numerical simulation of thermal cycle and void closing during friction stir spot welding of AA-2524 at different rotational speeds.*– Materials Characterization, vol.174, p.110984, doi.org/10.1016/j.matchar.2021.110984.
- [8] Hsieh M.J., Lee R.T. and Chiou Y.C. (2017): *Friction stir spot fusion welding of low-carbon steel to aluminum alloy.*– Journal of Materials Processing Technology, vol.240, pp.118-125, doi.org/10.1016/j.jmatprotec.2016.08.034.
- [9] Shen Z., Ding Y. and Gerlich A.P. (2020): *Advances in friction stir spot welding.*– Critical Reviews in Solid State and Materials Sciences, vol.45, No.6, pp.457-534.
- [10] Abdullah I.T. and Hussein S.K. (2018): *Improving the joint strength of the friction stir spot welding of carbon steel and copper using the design of experiments method.*– Multidiscipline Modeling in Materials and Structures, vol.14, No.5, pp.908-922.

- [11] Piccini J.M. and Svoboda H.G. (2015): *Effect of the tool penetration depth in Friction Stir Spot Welding (FSSW) of dissimilar aluminum alloys.*– Procedia Materials Science, vol.8, pp.868-877, doi.org/10.1016/j.mspro.2015.04.147.
- [12] Suryanarayanan R. and Sridhar, V.G. (2020): *Experimental investigation on the influence of process parameters in Friction stir spot welded dissimilar aluminum alloys.*– Materials Today: Proceedings, vol.27, No.1, pp.529-533, doi.org/10.1016/j.matpr.2019.11.319.
- [13] Akinlabi E.T., Osinubi A.S., Madushele N., Akinlabi S.A. and Ikumapayi O.M. (2020): *Data on microhardness and structural analysis of friction stir spot welded lap joints of AA5083-H116.*– Data in brief, vol.33, p.106585, doi.org/10.1016/j.dib.2020.106585.
- [14] Zhang G., Xiao C. and Ojo O. O. (2021): *Dissimilar friction stir spot welding of AA2024-T3/AA7075-T6 aluminum alloys under different welding parameters and media.*– Defence Technology, vol.17, No.2, pp.531-544, Apr. 2021, doi.org/10.1016/j.dt.2020.03.008.
- [15] Haribalaji V., Boopathi S. and Asif M. M. (2022): *Optimization of friction stir welding process to join dissimilar AA2014 and AA7075 aluminum alloys.*– Materials Today: Proceedings, vol.50, No.5, pp.2227-2234, doi.org/10.1016/j.matpr.2021.09.499.
- [16] Piccini J. M. and Svoboda H. G. (2015): *Effect of pin length on Friction Stir Spot Welding (FSSW) of dissimilar Aluminum-Steel joints.*– Procedia Materials Science, vol.9, pp.504-513, doi.org/10.1016/j.mspro.2015.05.023 .
- [17] Wang X., Morisada Y. and Fujii H. (2021): *Flat friction stir spot welding of low carbon steel by double side adjustable tools.*– Journal of Materials Science & Technology, vol.66, pp.1-9, doi.org/10.1016/j.jmst.2020.06.015.
- [18] Piccini J. M. and Svoboda H. G. (2017): *Tool geometry optimization in friction stir spot welding of Al-steel joints.*– Journal of Manufacturing Processes, vol.26, pp.142-154, doi.org/10.1016/j.jmapro.2017.02.004.
- [19] Garg A. and Bhattacharya A. (2017): *Similar and dissimilar joining of AA6061-T6 and copper by single and multi-spot friction stirring.*– Journal of Materials Processing Technology, vol.250, pp.330-344, doi.org/10.1016/j.jmatprotec.2017.07.029.
- [20] Tiwan, Ilman M.N., Kusmono. (2021): *Microstructure and mechanical properties of friction stir spot welded AA5052-H112 aluminum alloy.*– Heliyon, vol.7, No.2, p.e06009, doi.org/10.1016/j.heliyon.2021.e06009.
- [21] American Welding Society (1956): *Resistance Welding Theory and Use.*– Reinhold Publishing Corporation New York, Chapman & Hall, LTD, London.
- [22] American Society for Testing and Materials (ASTM) (1999): *Standard Practice for Microetching Metals and Alloys.*– ASTM E 407-99, Annual book of ASTM standards, vol.03.01.
- [23] Matsuda T., Hatano R., Ogura T., Suzuki R., Shoji H., Sano T. and Hirose, A. (2020): *Effect of mismatch in mechanical properties on interfacial strength of aluminum alloy/steel dissimilar joints.*– Materials Science and Engineering: A, vol.786, p.139437, doi.org/10.1016/j.msea.2020.139437.
- [24] Kumar C. L., Jayakumar V. and Bharathiraja G. (2019): *Optimization of welding parameters for friction stir spot welding of AA6062 with similar and dissimilar thicknesses.*– Materials Today: Proceedings, vol.19, No.2, pp.251-255, doi.org/10.1016/j.matpr.2019.07.204.
- [25] Yazdi S. R., Beidokhti B. and Haddad-Sabzevar M. (2019): *Pinless tool for FSSW of AA 6061-T6 aluminum alloy.*– Journal of Materials Processing Technology, vol.267, pp.44-51, doi.org/10.1016/j.jmatprotec.2018.12.005.
- [26] Suresh S., Venkatesan K., Natarajan E. and Rajesh, S. (2020): *Influence of tool rotational speed on the properties of friction stir spot welded AA7075-T6/Al₂O₃ composite joint.*– Materials Today: Proceedings, vol.27, pp.62-67, doi.org/10.1016/j.matpr.2019.08.220.
- [27] Matsuda T., Ogaki T., Hayashi K., Iwamoto C., Nozawa T., Ohata M. and Hirose A. (2022): *Fracture dominant in friction stir spot welded joint between 6061 aluminum alloy and galvanized steel based on microscale tensile testing.*– Materials & Design, vol.213, p.110344, doi.org/10.1016/j.matdes.2021.110344.

Received: June 23, 2022

Revised: October 29, 2022